High Frequency Autonomic Modulation: a new model for analysis of autonomic cardiac control

Pascal Champeroux, Pierre Fesler, Sébastien Judé, Serge Richard, Jean-Yves Le Guennec, Jérôme Thireau

High-frequency autonomic modulation: a new model for analysis of autonomic cardiac control

Correspondence Pascal Champéroux, Centre de Recherches Biologiques, CERB, Chemin de Montifault, Baugy 18800, France. E-mail: pascal.champeroux@cerb.fr

Pascal Champéroux[1], Pierre Fesler[2,3], Sebastien Judé[1], Serge Richard[1], Jean-Yves Le Guennec[3,*] and Jérôme Thireau[3,*]

[1]Centre de Recherches Biologiques, CERB, Baugy 18800, France, [2]Department of Internal Medicine, Hopital Lapeyronie, Montpellier, France, and [3]Laboratoire PHYMEDEXP,INSERM U1046, CNRS UMR 9214, Université de Montpellier, CHU Arnaud de Villeneuve, Montpellier Cedex 05 34295, France

*Equal contribution as senior authors.

BACKGROUND AND PURPOSE

Increase in high-frequency beat-to-beat heart rate oscillations by torsadogenic hERG blockers appears to be associated with signs of parasympathetic and sympathetic co-activation which cannot be assessed directly using classic methods of heart rate variability analysis. The present work aimed to find a translational model that would allow this particular state of the autonomic control of heart rate to be assessed.

EXPERIMENTAL APPROACH

High-frequency heart rate and heart period oscillations were analysed within discrete 10 s intervals in a cohort of 200 healthy human subjects. Results were compared to data collected in non-human primates and beagle dogs during pharmacological challenges and torsadogenic hERG blockers exposure, in 127 genotyped LQT1 patients on/off β-blocker treatment and in sub-groups of smoking and non-smoking subjects.

KEY RESULTS

Three states of autonomic modulation, S1 (parasympathetic predominance) to S3 (reciprocal parasympathetic withdrawal/sympathetic activation), were differentiated to build a new model of heart rate variability referred to as high-frequency autonomic modulation. The S2 state corresponded to a specific state during which both parasympathetic and sympathetic systems were coexisting or co-activated. S2 oscillations were proportionally increased by torsadogenic hERG-blocking drugs, whereas smoking caused an increase in S3 oscillations.

CONCLUSIONS AND IMPLICATIONS

The combined analysis of the magnitude of high-frequency heart rate and high-frequency heart period oscillations allows a refined assessment of heart rate autonomic modulation applicable to long-term ECG recordings and offers new approaches to assessment of the risk of sudden death both in terms of underlying mechanisms and sensitivity.

Abbreviations

ANS, autonomic nervous system; HF, high frequency; HFAM, high frequency autonomic modulation; HFHR, high-frequency heart rate oscillations; HFHRN, high-frequency heart rate oscillations in normalized units; HFRRN, high-frequency RR interval oscillations in normalized units; HFRR, high-frequency RR interval oscillations; HR, heart rate; HRV, heart rate variability; LF, low frequency

Introduction

The CNS regulates cardiac rhythm by modulating the activity and discharges of both limbs of the autonomic nervous system (ANS), that is, the sympathetic and parasympathetic pathways, at the level of pacemaker cells of the sinus node. As these nervous discharges are rhythmic, methods based on the analysis of heart rhythms have been proposed to assess the autonomic control of heart rate (HR) in a non-invasive manner from electrocardiographic (ECG) recordings (Billman, 2011). The parasympathetic nervous system is involved in faster rhythms than those driven by the sympathetic nervous system, based on their respective frequencies of nervous discharges (Akselrod *et al.*, 1981). Frequency-domain analysis methods are based on these frequency differences of heart rhythm oscillations. In humans, the standard threshold is fixed at 0.15 Hz (HRV Task Force, 1996), with rhythms above this threshold, that is, high-frequency (HF) rhythms, considered as having a parasympathetic origin while rhythms in the frequency range of 0.04–0.15 Hz, also named low-frequency (LF) rhythms, are thought to be of sympathetic origin. These rhythms are the main source of HR variability (HRV). HRV analysis in the frequency domain allows the partitioning of total HRV into frequency components, and power spectral analysis is used to quantify the power of LF and HF rhythms.

The two most common techniques of spectral analysis are fast Fourier transform analysis and autoregressive modelling. Based on these principles and techniques, the LF/HF ratio has been proposed as a gross index of sympatho-vagal balance. This parameter has become very popular both as a research tool for assessing autonomic control in human and animal studies and as an index for the risk of sudden death in various pathological contexts such as myocardial infarction (Tsuji *et al.*, 1996), heart failure (La Rovere *et al.*, 2003), stroke (Hilz *et al.*, 2011) and diabetes (Koivikko *et al.*, 2012). However, there is still some controversy regarding the partitioning of HRV in the frequency domain (Sammito and Böckelmann, 2016). Moreover, the LF band cannot be considered as reflecting rhythms with a sympathetic origin only (Parati *et al.*, 2006) but instead is strongly influenced by the parasympathetic component, leading to some surprising results, for instance, during treatment with β-adrenoceptor antagonists (β-blockers) or after myocardial infarction (HRV Task Force, 1996). Because LF and HF rhythms are rarely stationary except at rest, applying HRV analysis in the frequency domain to long-term ECG recordings is considered to have strong limitations. Since the publication of the HRV Task Force reference document, numerous publications on HRV have appeared and new methods of time and frequency domain analysis have been proposed. However, their contribution to the development of new clinical tools for the detection of high-risk patients is considered rather limited (Sassi *et al.*, 2015).

Paradoxically, spectral analysis of HRV consists of the analysis of the variability of the beat-to-beat heart period (RR interval) and not the beat-to-beat HR. Recently, the magnitude of HF beat-to-beat HR (HFHR) oscillations has been demonstrated as an interesting biomarker for the risk of drug-induced torsades de pointes (Champéroux *et al.*, 2015). Increases in HFHR oscillations induced by torsadogenic drugs were associated with signs of parasympathetic and sympathetic co-activation (Champéroux *et al.*, 2016). The present study aimed to design a model of autonomic cardiac modulation that would allow the assessment of parasympathetic and sympathetic co-activation.

Methods

Human ECGs

Twenty-four-hour Holter recordings (2/3-lead configuration, sampling rate: 200 Hz) were obtained from the Telemetric and Holter ECG Warehouse (THEW, hosted at the University of Rochester Medical Center, NY, USA), an initiative hosting a warehouse of digital Holter ECGs open to the scientific community. The E-HOL-03-0202-003 database of 200 healthy subjects [age > 15: 39 ± 16 (mean ± SD), 100 women, 100 men] was used to study HF oscillations in the healthy population. This database was also used to study influence of smoking on cardiac autonomic modulation (non-smoking, $n = 145$ vs. smoking, $n = 55$). Subjects were considered as eligible for enrolment and defined as healthy based on a battery of tests and information including no history of cardiovascular disease or disorders (stroke, TIAs and peripheral vascular disease), no history of high blood pressure (>150/90 mmHg), no medication, no chronic illness, normal physical examination, normal echocardiography, normal exercise testing and no pregnancy (Couderc, 2012). The E-HOL-03-0202-003 database refers to one Holter ECG recording per subject. The E-HOL-03-0480-013 database of genotyped LQTS patients was used to study HF oscillations under β-blocker treatment conditions in humans. The LQTS data were accumulated over 25 years and donated to the THEW by the Hospital Lariboisière (Paris, France). In the present work, 181 Holter recordings were analysed from 127 LQT1 patients [age > 15: 37 ± 15 (mean ± SD)]. All LQT1 patients were genotyped with mutations of the KCNQ1 subunit. Twenty-eight out of these 127 patients were recorded at successive ages of their life during on or off β-blocker treatment periods. From the 181 Holter recordings, 110 were collected from patients off β-blocker treatment and 71 from patients on β-blocker treatment.

Animal ECGs

Translational investigations were conducted in cynomolgus monkeys and beagle dogs to check the validity of the model across species. Twenty-four-hour telemetric ECG recordings were obtained in both species. All animal care and experimental procedures were subjected to ethical review (ethics committee no CEEA-111) according to European directive 2010/63/UE on animal welfare. Animal studies are reported in compliance with the ARRIVE guidelines (Kilkenny *et al.*, 2010; McGrath and Lilley, 2015). In accordance with the 3Rs encouraging the reduction in the number of animals used for experimental research, no animal experiments were specifically conducted for this study: only experiments recorded in the internal CERB database were re-analysed for this work.

All animal experiments were conducted in the conditions described below. Adult male and female (three males and three females per group) cynomolgus monkeys (3–7 kg, 28–48 months, Noveprim Ltd and Le Tamarinier, Republic

of Mauritius) and adult beagle dogs (10–15 kg, 8–24 months, CEDS, Mezilles, France) were fitted with radio telemetry transmitters (TL11M3D70PCTP or TL11M2D70PCT models, Data Sciences International, Saint Paul, MN, USA). Dogs were premedicated with acetylpromazine (0.05 mg·kg^{-1}, s.c.) and buprenorphine (0.01 mg·kg^{-1}, s.c.). Anaesthesia was induced by thiopental (15–20 mg·kg^{-1}, i.v.) and then maintained with isoflurane 0.5–1.5% in oxygen. Cynomolgus monkeys were premedicated with ketamine (10 mg·kg^{-1}, s.c.) buprenorphine (0.01 mg·kg^{-1}, s.c.) and meloxicam (0.1 mg·kg^{-1}, s.c.). Anaesthesia was induced by propofol (4–5 mg·kg^{-1}, i.v.) and halothane 4% and then maintained with halothane 1.5% in oxygen. After left thoracotomy, one electrode was sutured directly to the left ventricular epicardium near the apex while the second electrode was sutured to the pericardium above the right atrium to approximate a limb Lead II ECG. Analgesic treatment with buprenorphine/meloxicam was continued for a minimum of 2 days to alleviate any post-operative pain. A minimum period of 3 weeks was allowed for recovery from the surgery. Animals were housed in individual stainless steel cages for telemetry recordings. During the non-recording periods, dogs or cynomolgus monkeys were housed in pens or cages by groups of two to six animals at maximum with playing tools. Environmental parameters were recorded continuously and maintained within a fixed range, room temperature at 15–21°C for dogs and 20–24°C for cynomolgus monkeys, at 45–65% relative humidity for both species. The artificial day/night cycle was 12 h light and 12 h darkness with light on at 07:30 h. Drinking water was provided *ad libitum*. For beagle dogs, solid diet (300 g) was given daily in the morning. For cynomolgus monkeys, solid diet was given *ad libitum*, supplemented with fresh vegetables, fruits, bread and cereals. All dosing with drugs was performed between 15:00 and 15:30 h. ECGs were recorded continuously for a minimum of 2 h before dosing up to 24 h post dose. Animals serve as their own control according to an escalating dose design. Animals were dosed first with the vehicle of the reference pharmacological drug, then with the drug 48 to 72 h after the vehicle. Any 'period' effect was prevented by a training programme of animals to handling and dosing ensuring close baselines between dosing sessions. All animal experiments followed the same design. ECGs were recorded at a sampling rate of 500 Hz using ART™ acquisition software (Data Sciences International, St Paul, MN, USA).

Beat to beat analysis

Beat-to-beat HR and heart period (RR interval) values were calculated from an analysis of ECGs from lead II using software developed in RPL (RS/1 programming language, RS/1 release 6.3, Applied Materials). Ten-second sequences with the presence of arrhythmias or evidence of recording artefacts were automatically excluded from analysis. Sampling rates were increased to 1000 Hz using linear interpolation algorithms to prevent any jitter in the estimation of the R-wave fiducial point and risk of spectrum alteration (Pinna *et al.*, 1994; HRV Task Force, 1996).

HF oscillations of HR (HFHR) and heart period (HFRR)

The term 'HF oscillations' refers to the magnitude of beat-to-beat HR and heart period (RR interval) changes within discrete 10 s intervals. The magnitude of HF oscillations was calculated from the difference between the maximum and minimum beat-to-beat HR and RR interval values noted within each 10 s sequence, as previously described (Champéroux *et al.*, 2016).

The HFAM ratio

We observed that changes in HFHR oscillations were more sensitive to sympathetic blockade by atenolol than HFRR oscillations (Figure 1). We hypothesized that the relative influence of the two autonomic systems could be derived from the HFHR/HFRR ratio. Because the two variables (HFHR and HFRR) have different units, both parameters need to be the normalized. For this purpose, reference values for HF oscillations of the HR and RR interval, named $HFHR_{ref}$ and $HFRR_{ref}$, were determined in humans from 200 healthy subjects, cynomolgus monkeys (n = 77) and beagle dogs (n = 82). For monkeys and dogs, 'n' values refer to independent animals recorded in baseline conditions (treatment-free recording period) for 24 h. Data were collected over a period of 6 years

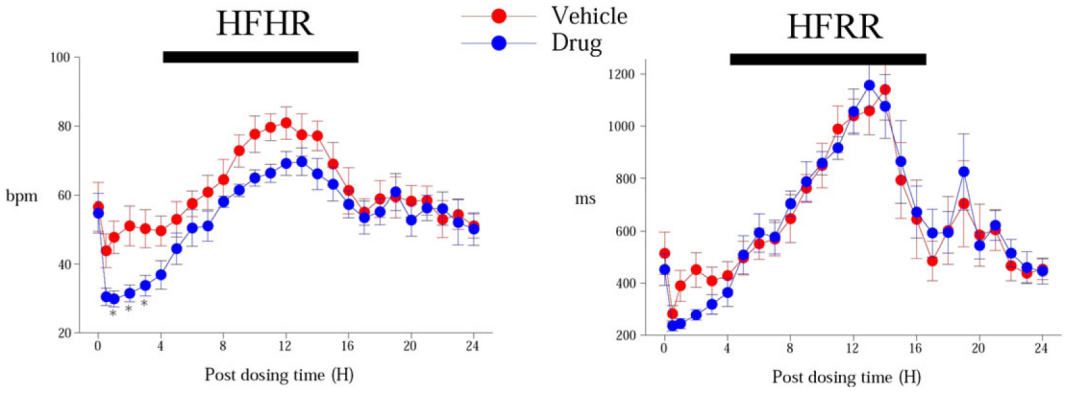

Figure 1

Effect of atenolol (1 mg·kg^{-1}, i.v.) on the magnitude of HFHR and HFRR oscillations in beagle dogs. The black bar represents the dark period of the 12 h light/12 h dark cycle. Data are presented as mean values ± SEM; n = 6. *$P \leq 0.05$, significantly different from vehicle.

(2010 to 2015). This database does not include any replicates of treatment-free recording period for any animals.

$HFHR_{ref}$ and $HFRR_{ref}$ values are rounded values from mean values which are calculated over the entire circadian period in each species, under baseline conditions (Table 1). More details about calculations of $HFHR_{ref}$ and $HFRR_{ref}$ values from distribution histograms of HFRR and HFHR oscillations in each species are given in Supporting Information Figure S1. Then, HFHR and HFRR oscillations were normalized (N) as follows:

HFHRN	HFHR/$HFHR_{ref}$ in normalized units
HFRRN	HFRR/$HFRR_{ref}$ in normalized units

The normalized oscillations ratio HFHRN/HFRRN was named the HF autonomic modulation (HFAM) ratio. Notably, the normalization of HF oscillations from mean circadian values allocates an equivalent weight for both variables and provides reference points from healthy subjects or animal population for the perspective of comparisons with drugs exposure conditions and risk factor analysis. Determination of HFRR and HFHR oscillations and calculations of HFRRN and HFHRN values and HFAM ratio are illustrated in the Figure 2 from three examples of ECG traces.

Power spectral analysis

RR interval values were re-sampled at a 1 Hz frequency. Power spectral analysis was obtained by applying a fast Fourier transform to successive and continuous 256 s sequences of 1-Hz re-sampled RR intervals. The power densities of LF and HF rhythms in ms^2 were derived from the integration of the power spectrum within the 0.04–0.15 Hz and 0.15–0.4 Hz frequency bands respectively (HRV Task Force, 1996). The LF/HF ratio was derived from the ratio of power densities of LF and HF rhythms and is considered by some investigators to mirror sympatho/vagal balance or to reflect sympathetic modulations (HRV Task Force, 1996).

Data and statistical analysis

The data and statistical analysis comply with the recommendations on experimental design and analysis in pharmacology (Curtis *et al.*, 2018). Operators for animal experiments and data analysts were not blinded. This work does not contain any subjective observation or analyses that would justify blinding. Furthermore, all calculations were made by using fully automated computer procedures (GLP validated) from beat-to-beat analysis of telemetry or Holter data up to statistics. Results are expressed as mean values ± SEM. The exact group size (n) is provided in legends of tables and figures (including the Supporting Information). 'n' values refer to independent animals or Holter recordings and not replicates. Values reported in graphs were calculated as 1 h reduced mean values to avoid the inclusion of aberrant values. Comparisons between groups were performed using a repeated measures ANOVA, followed by a Dunnett's test when there was statistically significant 'Group' difference or 'Group X Time' interaction. The level of probability (P) deemed to constitute the threshold for statistical significance was fixed at $P \leq 0.05$. Statistics were carried out using RS/1 release 6.3, Applied Materials.

Table 1

$HFHR_{ref}$ and $HFRR_{ref}$ values in humans, cynomolgus monkeys and beagle dogs

Species	$HFHR_{ref}$ (bpm)	$HFRR_{ref}$ (ms)
Human	10	110
Cynomolgus	20	90
Beagle dogs	70	700

$HFHR_{ref}$ and $HFRR_{ref}$ values derived from mean HFHR and HFRR values over the entire circadian cycle in human subjects (n = 200), cynomolgus monkeys (n = 77) and beagle dogs (n = 82).

Materials

Atenolol, **atropine** sulphate or methyl-nitrate, **cisapride**, **clonidine** hydrochloride, **haloperidol** and **thioridazine** were purchased from Sigma-Aldrich (Saint Quentin, France). **Dofetilide** was purchased from Sequoia Research Product Ltd (United Kingdom). Drugs were dissolved in sterile saline or water.

Nomenclature of targets and ligands

Key protein targets and ligands in this article are hyperlinked to corresponding entries in http://www.guidetopharmacology.org, the common portal for data from the IUPHAR/BPS Guide to PHARMACOLOGY (Harding *et al.*, 2018), and are permanently archived in the Concise Guide to PHARMACOLOGY 2017/18 (Alexander *et al.*, a, b).

Results

Changes in mean HR in all analyses presented in this work are reported in the Supporting Information.

Characterization of the three states of the autonomic modulation in the HF band

The pattern of HF oscillations within 10 s sequences was inspected according to HFHRN/HFRRN values and magnitude of HFHRN and HFRRN oscillations in humans, cynomolgus monkeys and beagle dogs. We differentiated three patterns characterized respectively by (S1) stable, fast and large HFRR and HFHR oscillations (Figure 2A), (S2) unstable and partially blunted fast oscillations within 10 s sequences (Figures 2B), and (S3) stable and more or less blunted HFRR and HFHR oscillations (Figure 2C).

Discrete algorithms were then designed to automatically identify each state. For the first pattern, normalized HFRR oscillations were larger than HFHR oscillations. This state was named S1. The corresponding S1 algorithm was defined as follows: HFHRN/HFRRN≤1.

In contrast to S1, the second pattern, named S2, showed non-stationary and partially blunted fast oscillations within 10 s sequences. Non-stationarity was characterized by the presence of fast oscillations partially blunted and replaced by slower and more or less large phases of acceleration or deceleration within the 10 s sequences. In this state, normalized HFHR values were greater than 1. The S2 algorithm was defined as follows: HFHRN/HFRRN>1and HFHRN>1.

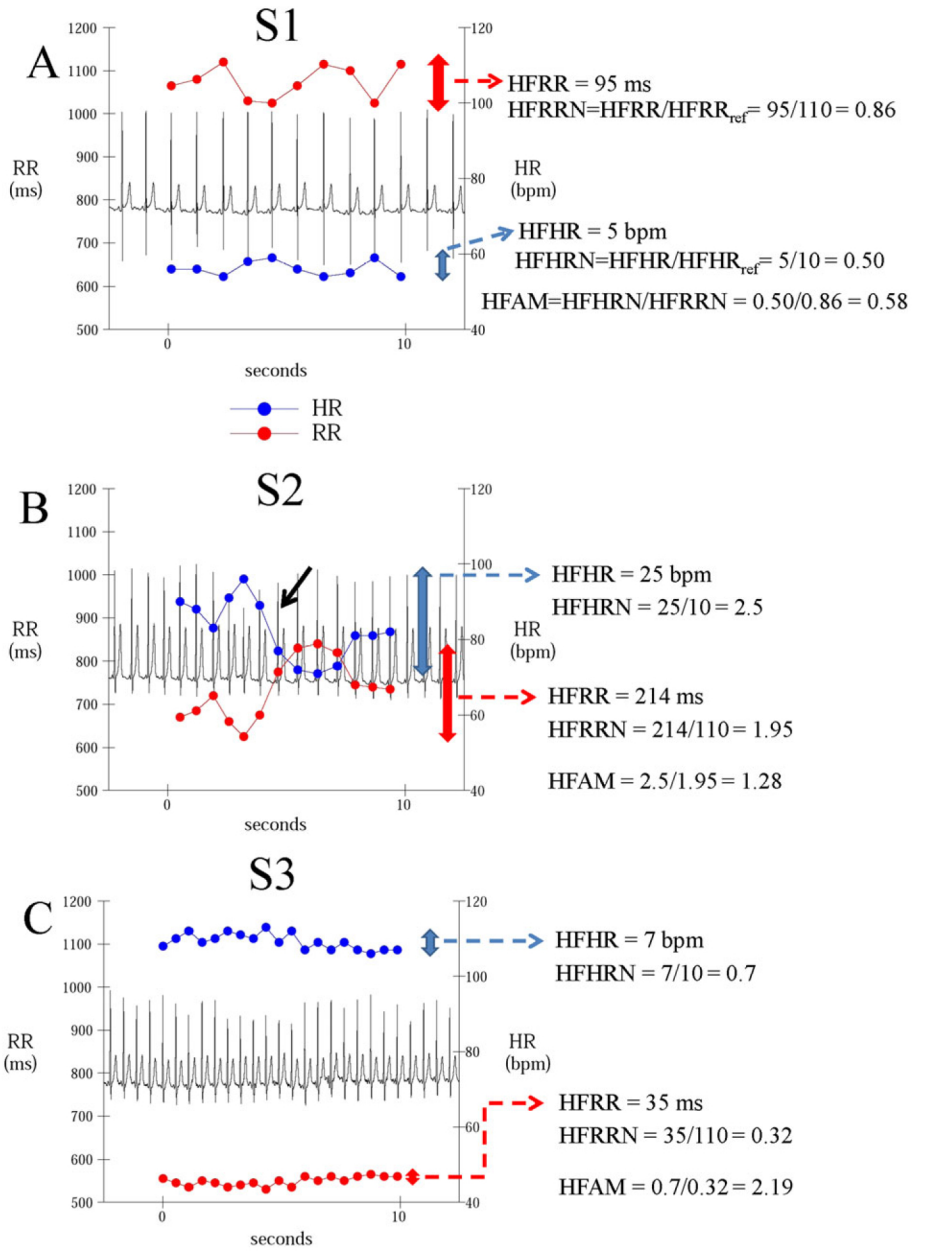

Figure 2

Typical ECG traces and HFHR and HFRR oscillations depicting the three states of the HFAM model. ECG traces were recorded in a 22-year-old woman. S1: stable, fast and large oscillations. S2: non-stationary and partially blunted fast oscillations inside 10 s sequences. Fast parasympathetic oscillations are partially blunted and replaced by slower phases of acceleration/deceleration (indicated by black arrows) inside the 10 s sequence. S3: Both HFRR and HFHR oscillations are blunted. Blue and red arrows: magnitude of HFHR and HFRR oscillations respectively. Details of calculations of the HFAM ratio are provided in parallel.

For the third pattern, S3, HFRR and HFHR oscillations were stationary and blunted when compared with S1 oscillations. As a consequence of the blunting of HF oscillations, they were characterized by normalized HFRR and HFHR values less than 1. Consequently, the S3 algorithm was defined as follows: HFHRN/HFRRN>1 and HFHRN<1.

It is worth noting that these three algorithms are complementary and allow the classification of all analysed 10 s sequences in the proposed model.

Applying the HFAM model to the circadian cycle across species

The HFAM model was first used to analyse the circadian cycle in humans, cynomolgus monkeys and beagle dogs (Figure 3). As expected, S1 oscillations appeared to predominate in all species during the night and were associated with an increase in the HFAM ratio. Conversely, the HFAM ratio was increased during the diurnal period. Likewise, S2 and S3 oscillations were proportionally increased during the light period, except

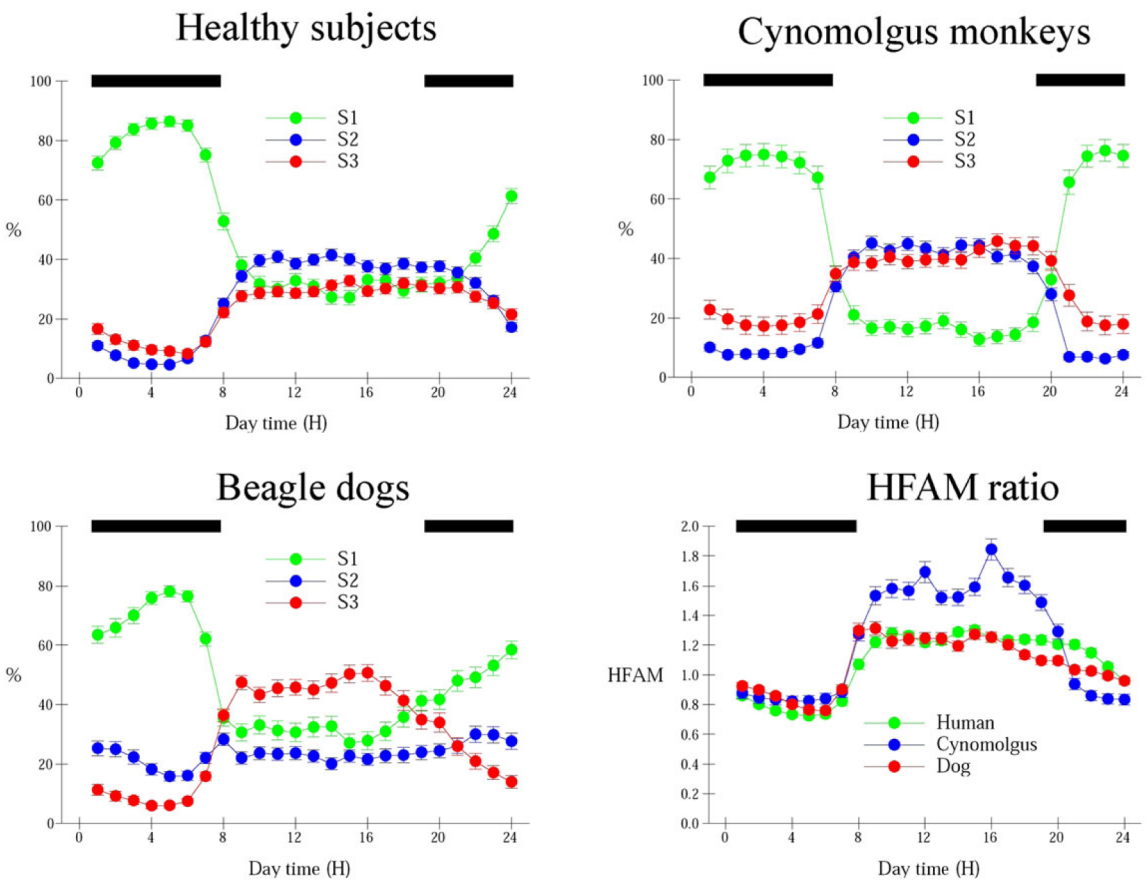

Figure 3

Changes in S1, S2 and S3 oscillations and in the HFAM ratio over the circadian cycle in healthy subjects (n = 200), cynomolgus monkeys (n = 77) and beagle dogs (n = 82). Data shown are means ± SEM. Ratios are expressed as %·h^{-1}. The black bar represents the dark period of the 12 h light/12 h dark cycle.

S2 oscillations in dogs which remained relatively similar between dark and light periods. These results provide the first evidence of the good translation of the HFAM model between species, despite noticeable differences in HR baseline and huge differences between the magnitude of HF oscillations in primates and dogs. These results also show that the HFAM model is more than a simple static reflection of HR, as it is capable of distinguishing different ANS influences on cardiac rhythm.

Pharmacological characterization of the HFAM model in non-human primates and dogs

Analysis of effects induced by several pharmacological agents (atenolol, to provide **β_1-adrenoceptor** blockade; atropine, to provide **muscarinic** receptor blockade; clonidine, to provide central sympathetic inhibition and parasympathetic stimulation) were used to characterize the S1, S2 and S3 states both in cynomolgus monkeys and beagle dogs (Figure 4). Full graphs over the 24 h period following dosing are presented as Supporting Information Figures S1–S3 for cynomolgus monkeys and Supporting Information Figures S4–S6 for beagle dogs.

These analyses confirm that S1 oscillations are large and pure parasympathetic oscillations as they were not reduced by acute dosing with atenolol but abolished under conditions of parasympathetic blockade, with atropine. Consistent with these findings, S1 oscillations were markedly increased by clonidine, a central parasympathomimetic/sympatholytic agent. Under atenolol, S1 oscillations were even slightly increased due to a shift in autonomic modulation in favour of S1 oscillations, due to the suppression of S2 oscillations during the light period. S2 oscillations are related to parasympathetic and sympathetic co-activation as they disappeared, equally, under conditions of either sympathetic inhibition (atenolol, clonidine) or parasympathetic blockade (atropine). S3 oscillations reflect reciprocal sympathetic activation and/or parasympathetic withdrawal associated with reduced HRV (blunted HF oscillations) as they were markedly increased under conditions of parasympathetic blockade (atropine) due to reciprocal sympathetic activation. Consistent with these results, the S3 state was either unchanged by sympathetic blockade by atenolol (reflecting an absence of sympathetic excitation under basal conditions) or reduced by clonidine under conditions of parasympathetic stimulation, due to a shift towards S1 oscillations. Accordingly, changes in the HFAM ratio consistently reflect global autonomic

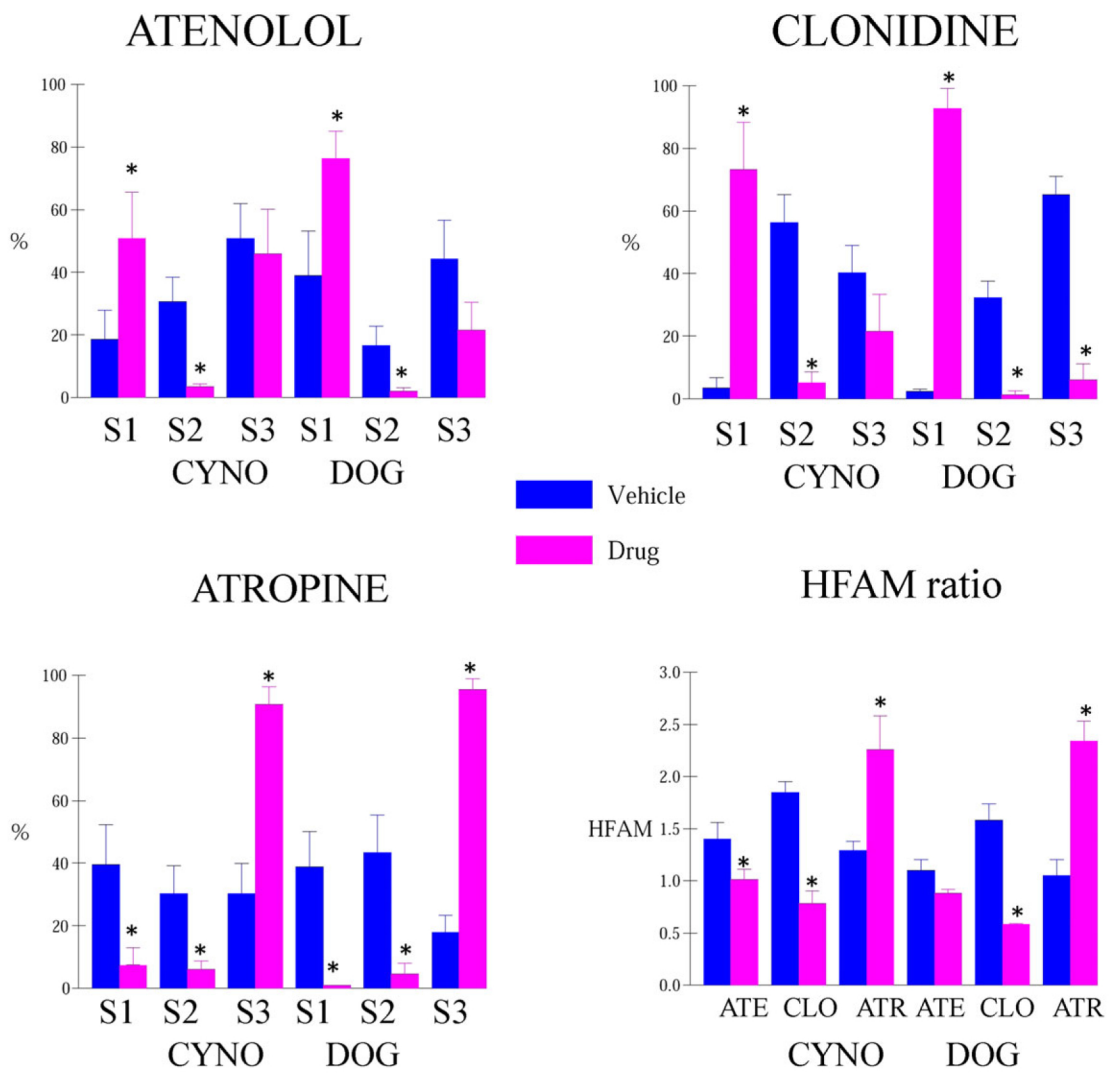

Figure 4

Pharmacological characterization of the HFAM model in non-human primates and beagle dogs. Effects of atenolol (ATE; 1 mg·kg^{-1}, i.v., 2 h after dosing (p.d.) in cynomolgus (CYNO) and 6 h p.d. in dogs), clonidine (CLO; 30 μg·kg^{-1}, i.v., 1 h p.d. in cynomolgus and 2 h p.d. in dogs) and atropine (ATR; 1 mg·kg^{-1}, i.v., 1 h p.d. in cynomolgus and 12 h p.d. in dogs) on S1, S2 and S3 oscillations and on the HFAM ratio in cynomolgus monkeys and beagle dogs (n = 6 per group). Data shown are means ± SEM. Ratios are expressed as %·h^{-1}. *$P \leq 0.05$, significantly different from vehicle.

modulation in favour of a lowering of the sympathetic influence in the presence of atenolol, parasympathetic predominance in the presence of clonidine or a reciprocal sympathetic activation/parasympathetic withdrawal in the presence of atropine.

Translation of the HFAM model to humans

The translation of the HFAM model to humans was studied by comparing smoking versus non-smoking subgroups of subjects and by analysing the effects of β-blocker treatment in LQT1 patients.

In smoking subjects, S2 oscillations remained unchanged when compared to non-smoking subjects (Figure 5). Smoking caused a shift in autonomic modulation in favour of S3 oscillations to the detriment of S1 oscillations. An increase in the HFAM ratio reflects a parasympathetic withdrawal and/or sympathetic activation. Interestingly, the HFAM model demonstrates that these effects persisted, even during non-smoking periods such as the night, suggesting a resetting of the autonomic modulation towards lower parasympathetic activity and/or higher sympathetic activity in smokers.

Applying the HFAM model to LQT1 patients showed that β-blocker treatment caused a shift in autonomic modulation in favour of S1 oscillations to the detriment of S3 oscillations (Figure 6). S2 oscillations were largely reduced during the light period only, confirming the strong contribution of the sympathetic nervous system to this autonomic state in humans. The lowering of the HFAM ratio reflects higher parasympathetic modulation, as previously reported under β-blocker treatment in patients, following acute myocardial infarction (Sandrone *et al.*, 1994).

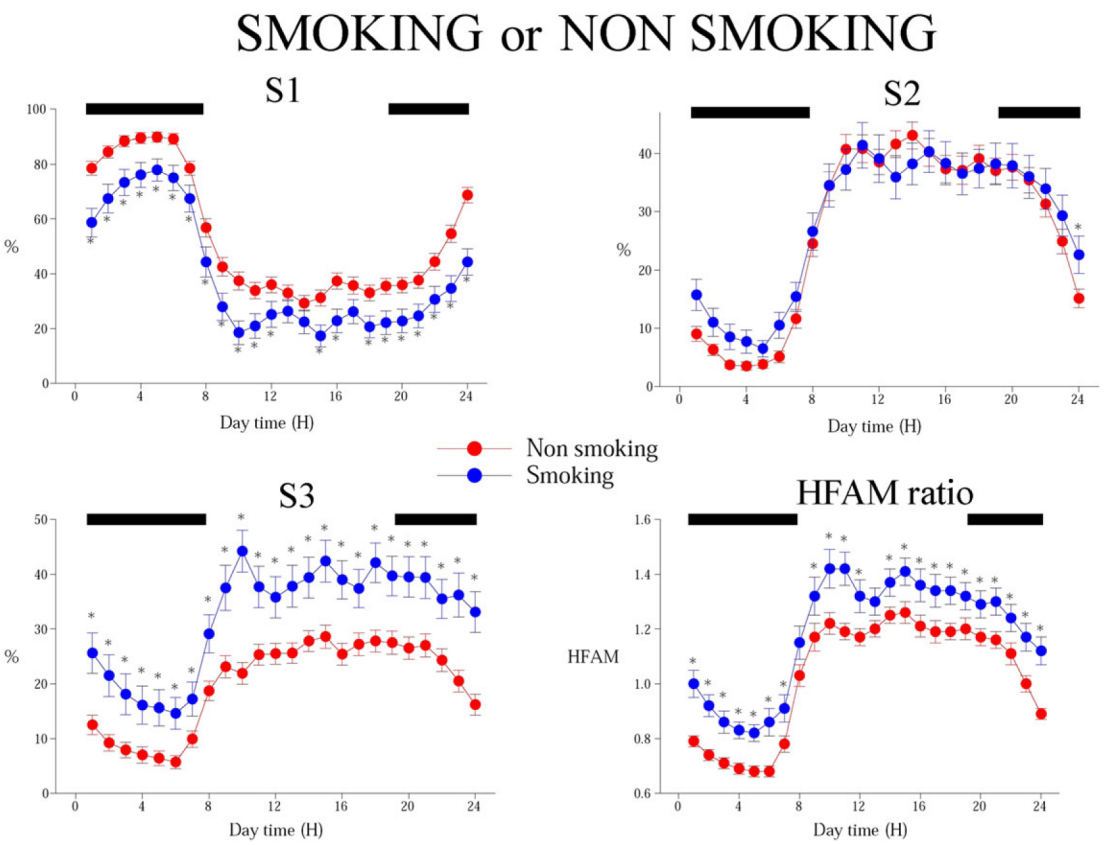

Figure 5

Comparison of smoking (n = 55) with non-smoking (n = 145) subjects. The HFAM model shows an increase in S3 oscillations throughout the circadian cycle, confirming the good translation of the HFAM model to humans in the context of parasympathetic withdrawal and/or sympathetic activation. Data shown are means ± SEM. Ratios are expressed as %·h^{-1}. The black bar represents the dark period of the 12 h light/12 h dark cycle. *$P \leq 0.05$, significantly different from non-smoking.

Taken together, these results confirm the good translation of the HFAM model to humans in contexts of sympathetic inhibition and activation. We compared the HFAM model with a standard power spectral HRV analysis. Power spectral analysis (Figure 7) confirms changes in autonomic balance in LQT1 patients through LF/HF ratio analysis in the context of sympathetic inhibition, but the LF/HF ratio fails to demonstrate statistically significant changes in the autonomic balance in smokers, as previously reported (Lucini *et al.*, 1998). Moreover, the significant contribution to parasympathetic rhythms in the LF band makes it difficult to interpret changes in sympathetic rhythms when considering changes in LF and HF rhythms alone, in both contexts of sympathetic inhibition and activation.

Arrhythmic blockers of hERG channels

Torsadogenic drugs that block **hERG channels**, proportionally increased S2 oscillations (Figure 8) confirming that these arrhythmic agents cause the co-activation of both limbs of the ANS. Full graphs over the 24 h period following dosing are presented as Supporting Information Figures S7–S10.

Discussion

This work demonstrates that analysis of the magnitude of the HR and heart period oscillations within discrete 10 s intervals, enables the differentiation of discrete states of autonomic modulation. Direct recordings of the activities of the sympathetic stellate ganglion nerve and the thoracic vagal nerve in dogs by telemetry demonstrated few circadian changes in parasympathetic activity whereas sympathetic activity was increased during the light period (Ogawa *et al.*, 2007). Accordingly, the HFAM model reflects autonomic modulation during the circadian cycle, as parasympathetic S1 oscillations predominate during the night whereas autonomic modulation depends on changes in sympathetic activity resulting from complex interactions between both limbs of the ANS during the light period. During the diurnal period, the HFAM model differentiated between two further types of autonomic modulation. The best known interaction is characterized by S3 oscillations that reflect sustained reciprocal influence between the two systems, leading to reduced HRV. Alternatively, this reciprocal modulation can be transitory and very short-lived leading to non-stationary oscillations. The latter mode is shown as S2 oscillations during which both fast parasympathetic oscillations and blunted oscillations are

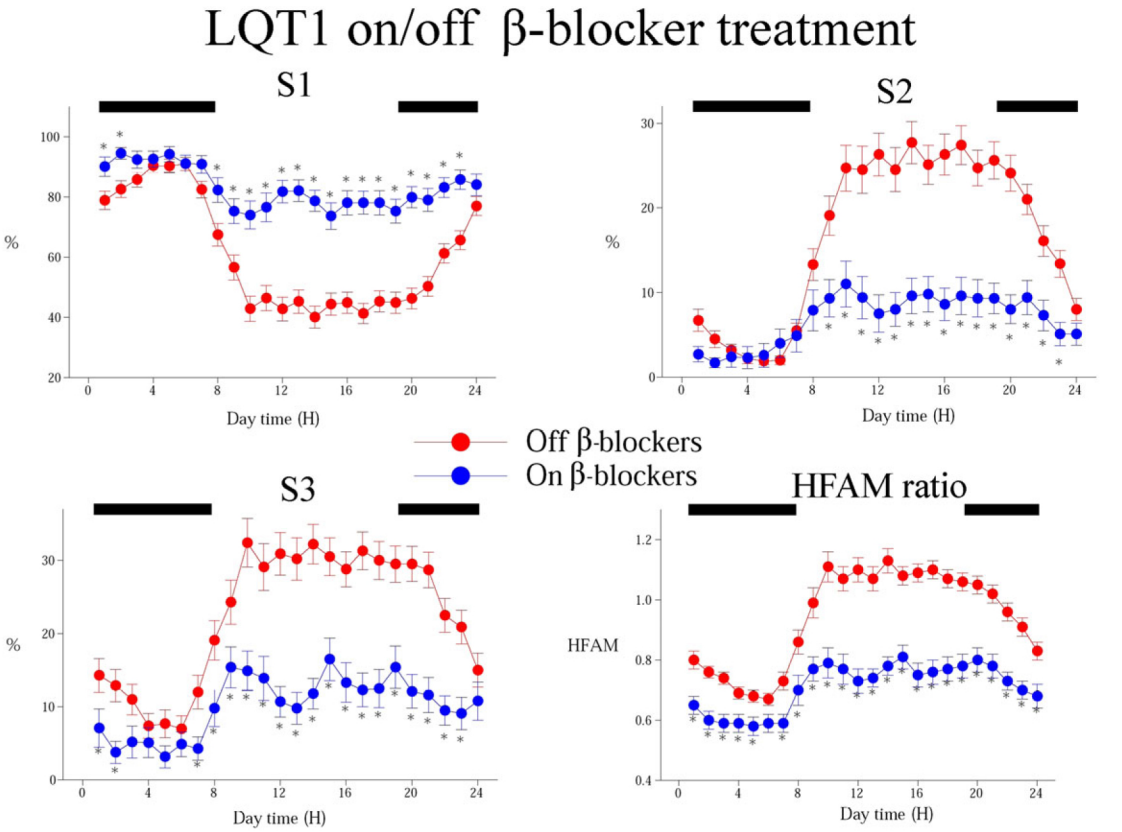

Figure 6

The HFAM model applied to LQT1 patients on or off β-blocker treatment (110 Holter recordings in patients off β-blocker treatment and 71 Holter recordings in patients on β-blocker treatment). β-blocker treatment in LQT1 patients causes a shift of autonomic control in favour of S1 oscillations to the detriment of all other oscillations of the HFAM model, confirming the good translation of the model to humans in the context of sympathetic inhibition. Data shown are means ± SEM. Ratios are expressed as $\%\cdot h^{-1}$. The black bar represents the dark period of the 12 h light/12 h dark cycle. *$P \leq 0.05$, significantly different from off treatment.

present within short 10 s sequences. The choice of a 10 s window corresponds to a slight enlargement of the HF oscillation window, which should have been fixed at 6 s when considering the low conventional limit of the HF frequency band: 0.15 Hz. Within this 10 s window, the HFAM model facilitates the exploration of the influence of slow sympathetic rhythms (LF) on the magnitude of HF oscillations. In the context of parasympathetic withdrawal and reciprocal sympathetic activation, HRV is known to be reduced because of the blunting of HF oscillations (Billman, 2011). Accordingly, HFHRN and HFRRN oscillations are lowered. In such a context, the decrease in HFRRN oscillations is more important than that of HFHRN oscillations. In this situation of sympathetic activation, the HFAM model exhibits similarities, through the HFHRN/HFRRN ratio, with the LF/HF ratio. Indeed, in this context, both HF and LF rhythms are reduced, but the lowering of HF rhythms is more pronounced than that of LF rhythms, explaining the increase of the LF/HF ratio.

The HFAM model demonstrates that the proportion of non-stationary S2 oscillations is important during the diurnal period, about 20–40% depending on species. This finding confirms that the probability that autonomic rhythms are stationary over the 5 min recording sequences required to apply power spectral analysis is low in long-term ECG recordings (HRV Task Force, 1996). This lack of "stationarity" is enhanced by uncontrolled breathing conditions in long-term ECG recordings. To counteract this source of variability, it is recommended that ECGs are recorded at rest under controlled respiration conditions over 5 min periods for HRV assessment (Brown *et al.*, 1993). These conditions cannot be attained in animal studies (telemetry) or during 24 h Holter recordings in humans, making it difficult to interpret data from such recordings and causing further inconsistencies in the analysis of autonomic modulation (Billman, 2011). Conversely, the HFAM model significantly improves the interpretation of autonomic modulation under long-term ECG recording conditions by taking into account periods during which autonomic rhythms are not stationary (S2) due to the co-existence of sympathetic and parasympathetic activities. Alternatively, the HFAM model provides a probabilistic assessment of autonomic modulation through an analysis of the proportion between the three states S1 to S3, rather than a quantitative measure of sympatho-vagal balance. The latter aspect can nevertheless be appreciated through the HFHRN/HFRRN (HFAM) ratio with improved sensitivity when compared with the LF/HF ratio.

The co-activation or co-existence with activation of one or both components of the ANS has been reported in various

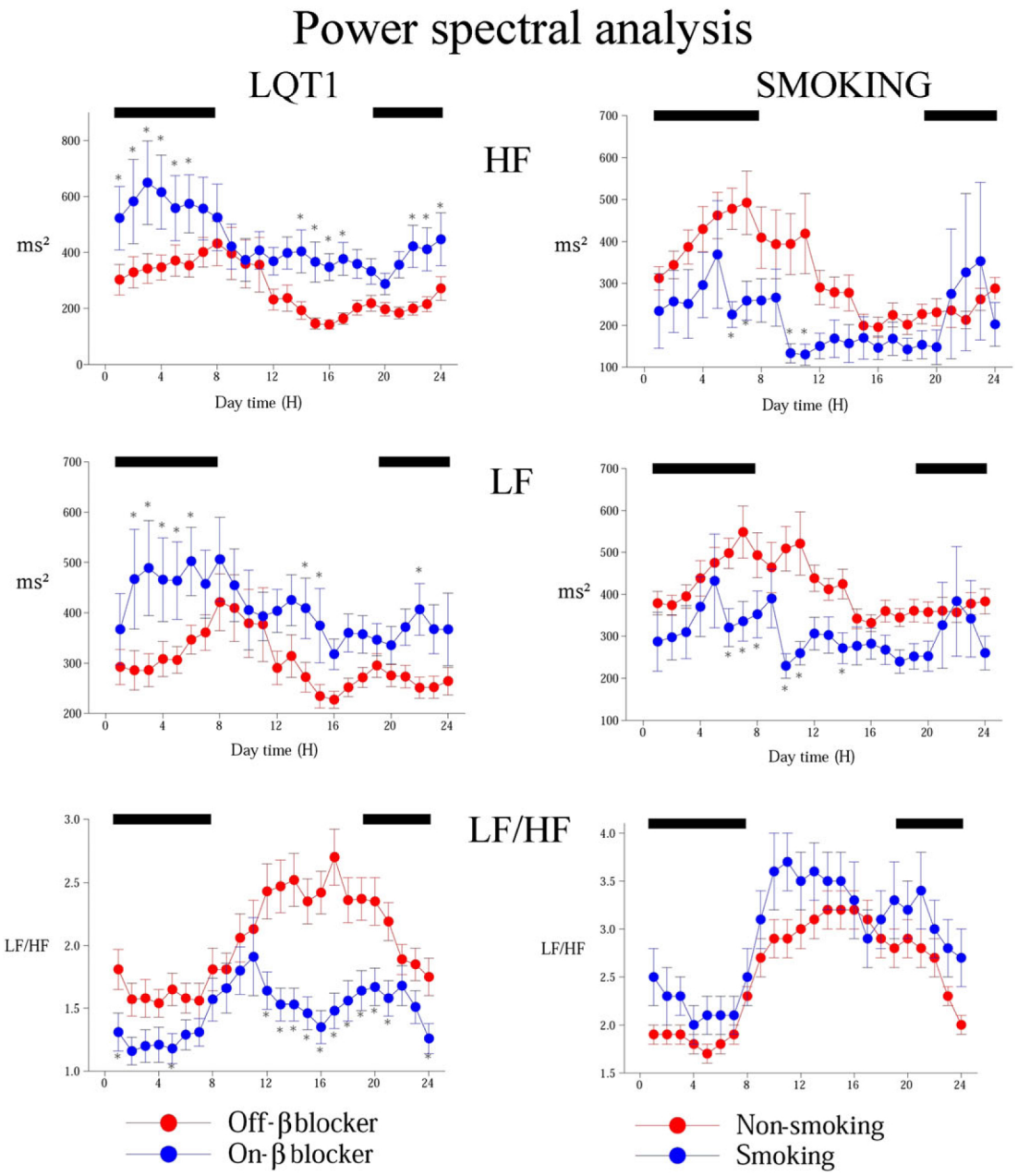

Figure 7

Applying power spectral analysis to LQT1 patients on/off β-blocker treatment (110 Holter recordings in patients off β-blocker treatment and 71 Holter recordings in patients on β-blocker treatment), and in non-smoking (n = 145) and smoking subjects (n = 55). Except for changes in the LF/HF ratio in LQT1 patients, a clear interpretation of the autonomic modulation is rather difficult in both LQT1 patients and smoking subjects. Data shown are means ± SEM. The black bar represents the dark period of the 12 h light/12 h dark cycle. *$P \leq 0.05$, significant effects of β-blocker or smoking.

situations such as during mild baroreflex sympathetic activation (Berntson *et al.*, 1991), during sudden emotional stress (Iwata and Le Doux, 1988), following nociceptive stimulation (Chouchou *et al.*, 2011), or during the post-exercise phase due to the persistence of the sympathetic metaboreflex (Iellamo *et al.*, 1999) and LF rhythms overlapping the post-exercise parasympathetic-mediated slowing of the heart rhythm. Although further work is needed to characterize in detail each of these situations, they are likely to represent the majority of S2 oscillations as they are more prominent during the diurnal period and are markedly reduced by β-blocker treatment. However, stochastic non-stationary events cannot be excluded in this S2 state, although they would be largely in the minority as these S2 oscillations are not abolished by β-blocker treatment in LQT1 patients. Interestingly, some of these situations (emotional stress, exercise) have been reported to be triggers of arrhythmic events in a large proportion of LQT2 patients with hERG channel

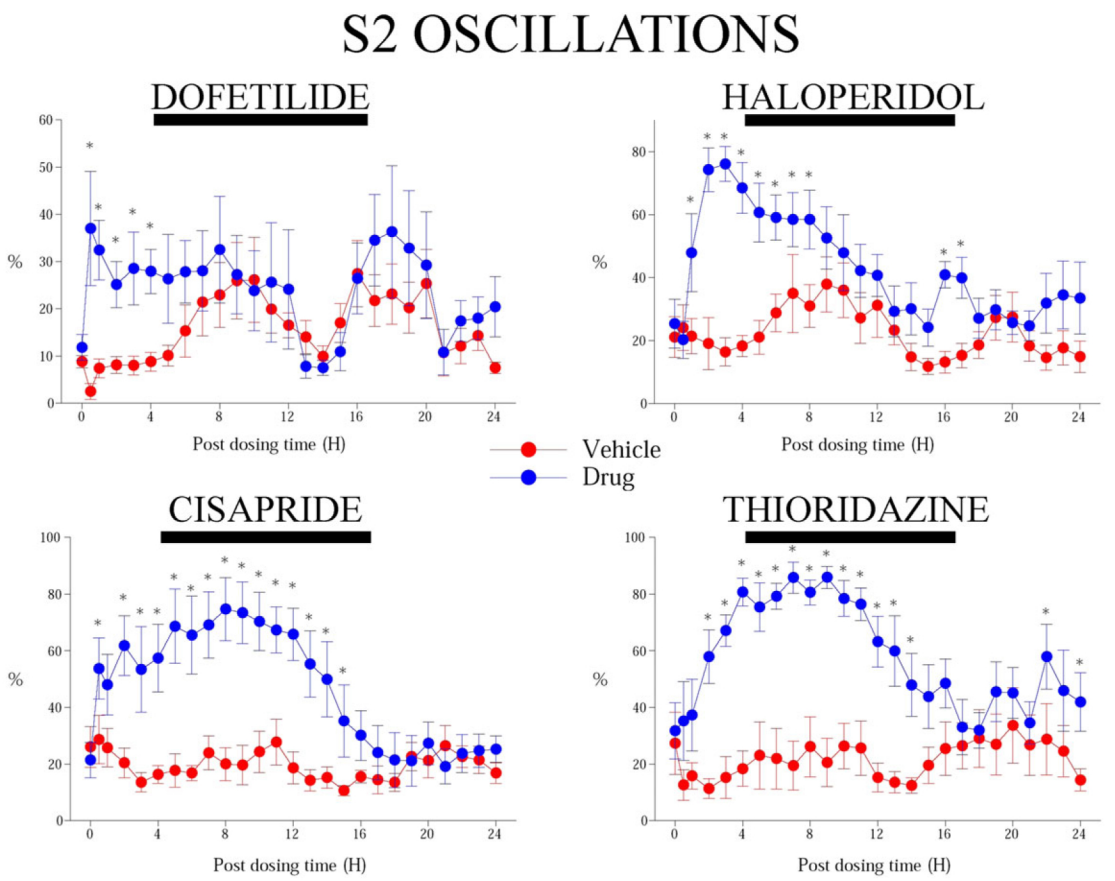

Figure 8

Effect of dofetilide (1 mg·kg^{-1}, p.o.), haloperidol (3 mg·kg^{-1}, p.o.), cisapride (6 mg·kg^{-1}, p.o.) and thioridazine (1.5 mg·kg^{-1}, p.o.) on S2 oscillations ratios (%·h^{-1}) in beagle dogs. The black bar represents the dark period of the 12 h light/12 h dark cycle. Data are presented as mean values ± SEM (n = 6). *$P \leq 0.05$, significantly different from vehicle.

mutations (Kim *et al.*, 2010). Likewise, several hERG-blocking drugs (e.g. dofetilide, thioridazine) known for their association with torsades de pointes in humans have been demonstrated to increase HFHR oscillations in animal studies (Champéroux *et al.*, 2015) which in turn increased the beat-to-beat ventricular repolarisation variability, a situation that favours occurrence of torsades de pointes (Champéroux *et al.*, 2016). The present study shows that these arrhythmic drugs cause increases in the proportion of S2 oscillations, also confirming the co-activation of both limbs of the ANS and providing an explanation for the increases in HFHR oscillations described previously with these drugs. However, the predictive value as a risk factor in human disease contexts remains to be demonstrated for S2 oscillations since the risk of sudden death is currently and generally associated with reduced HRV and elevated sympathetic activity. Nevertheless, our study demonstrates an improved sensitivity for detection of reduced HRV through an increase in S3 combined with an increase in the HFAM ratio when compared to spectral analysis in smoking subjects, which offers good diagnostic prospects in this context too.

In conclusion, the HFAM model allows, for the first time, assessment of a specific state of the autonomic control of HR, characterized by co-existence or co-activation of both components of the ANS. Moreover, this model allows a sensitive and refined estimation of the HR autonomic modulation applicable to long-term ECG recordings analysis and offers new approaches to the assessment of the risk of sudden death, both in terms of the underlying mechanisms and in terms of sensitivity.

Acknowledgement

We thank Dr. S. Rasika of Gap Junction (www.gapjunction.com) for assistance with English editing.

Author contributions

The HFAM model was designed by P.C. Data analysis was performed by P.C. Manuscript was written by P.C., J.T. and J.Y.L. and critically evaluated by P.F., S.J. and S.R.

Conflict of interest

The authors declare no conflicts of interest.

Declaration of transparency and scientific rigour

This Declaration acknowledges that this paper adheres to the principles for transparent reporting and scientific rigour of preclinical research recommended by funding agencies, publishers and other organisations engaged with supporting research.

References

Akselrod S, Gordon D, Ubel FA, Shannon DC, Barger AC, Cohen RJ (1981). Power spectrum analysis of heart rate fluctuations: a quantitative probe of beat-to-beat cardiovascular control. Science 213: 220–222.

Alexander SPH, Striessnig J, Kelly E, Marrion NV, Peters JA, Faccenda E *et al.* (2017a). The Concise Guide to PHARMACOLOGY 2017/18: Voltage-gated ion channels. Br J Pharmacol 174: S160–S194.

Alexander SPH, Christopoulos A, Davenport AP, Kelly E, Marrion NV, Peters JA *et al.* (2017b). The Concise Guide to PHARMACOLOGY 2017/18: G protein-coupled receptors. Br J Pharmacol 174: S17–S129.

Berntson GG, Cacioppo JT, Quigley KS (1991). Autonomic determinism: the modes of autonomic control, the doctrine of autonomic space, and the laws of autonomic constraint. Psychol Rev 98: 459–487.

Billman GE (2011). Heart rate variability – a historical perspective. Front Physiol 2: 1–13.

Brown TE, Beightol LA, Koh J, Eckberg DL (1993). Important influence of respiration on human R-R interval power spectra is largely ignored. J Appl Physiol 75: 2310–2317.

Champéroux P, Le Guennec JY, Jude S, Laigot C, Maurin A, Sola ML *et al.* (2016). The high frequency relationship: implications for torsadogenic hERG blockers. Br J Pharmacol 173: 601–612.

Champéroux P, Thireau J, Jude S, Laigot-Barbé C, Maurin A, Sola ML *et al.* (2015). Dofetilide induced QT interval short term variability and ventricular arrhythmias are dependent on high frequency autonomic oscillations. Br J Pharmacol 172: 2878–2891.

Chouchou F, Pichot V, Perchet C, Legrain V, Garcia-Larrea L, Roche F *et al.* (2011). Autonomic pain responses during sleep: a study of heart rate variability. Eur J Pain 15: 554–560.

Couderc JP (2012). The Telemetric and Holter ECG Warehouse (THEW): the first three years of development and research. J Electrocardiol 45: 677–683.

Curtis MJ, Alexander S, Cirino G, Docherty JR, George CH, Giembycz MA *et al.* (2018). Experimental design and analysis and their reporting II: updated and simplified guidance for authors and peer reviewers. Brit J Pharmacol 175: 987–993.

Harding SD, Sharman JL, Faccenda E, Southan C, Pawson AJ, Ireland S *et al.* (2018). The IUPHAR/BPS Guide to PHARMACOLOGY in 2018: updates and expansion to encompass the new guide to IMMUNOPHARMACOLOGY. Nucl Acids Res 46: D1091–D1106.

Hilz MJ, Moeller S, Akhundova A, Marthol H, Pauli E, De Fina P *et al.* (2011). High NIHSS values predict impairment of cardiovascular autonomic control. Stroke 42: 1528–1533.

Iellamo F, Pizzinelli P, Massaro M, Raimondi G, Peruzzi G, Legramante JM (1999). Muscle metaboreflex contribution to sinus node regulation during static exercise: insights from spectral analysis of heart rate variability. Circulation 100: 27–32.

Iwata J, Le Doux JE (1988). Dissociation of associative and nonassociative concomitants of classical fear conditioning in the freely behaving rat. Behav Neurosci 102: 66–76.

Kilkenny C, Browne W, Cuthill IC, Emerson M, Altman DG (2010). NC3Rs reporting guidelines working group. Animal research: reporting in vivo experiments: the ARRIVE guidelines. Br J Pharmacol 160: 1577–1579.

Kim JA, Lopes CM, Moss AJ, McNitt S, Barsheshet A, Robinson JL *et al.* (2010). Trigger-specific risk factors and response to therapy in long QT syndrome type 2. Heart Rhythm 7: 1797–1805.

Koivikko ML, Tulppo MP, Kiviniemi AM, Kallio MA, Perkiömäki JS, Salmela PI *et al.* (2012). Autonomic cardiac regulation during spontaneous nocturnal hypoglycemia in patients with type 1 diabetes. Diabetes Care 35: 1585–1590.

La Rovere MT, Pinna GD, Maestri R, Mortara A, Capomolla S, Febo O *et al.* (2003). Short-term heart rate variability strongly predicts sudden cardiac death in chronic heart failure patients. Circulation 107: 565–570.

Lucini D, Bertocchi F, Malliani A, Pagani M (1998). Autonomic effects of nicotine patch administration in habitual cigarette smokers: a double-blind, placebo-controlled study using spectral analysis of RR interval and systolic arterial pressure variabilities. J Cardiovasc Pharmacol 31: 714–720.

McGrath JC, Lilley E (2015). Implementing guidelines on reporting research using animals (ARRIVE etc.): new requirements for publication in BJP. Br J Pharmacol 172: 3189–3193.

Ogawa M, Zhou S, Tan AY, Song J, Gholmieh G, Fishbein MC *et al.* (2007). Left stellate ganglion and vagal nerve activity and cardiac arrhythmias in ambulatory dogs with pacing-induced congestive heart failure. J Am Coll Cardiol 50: 335–343.

Parati G, diRienzo M, Castiglioni P, Mancia G, Taylor JA, Studinger P (2006). Point: counterpoint: cardiovascular variability is/is not an index of autonomic control of circulation. J Appl Physiol 101: 676–682.

Pinna GD, Maestri R, Di Cesare A, Colombo R, Minuco G (1994). The accuracy of power-spectrum analysis of heart-rate variability from annotated RR list generated by Holter systems. Physiol Meas 15: 163–179.

Sammito S, Böckelmann I (2016). Reference values for time- and frequency-domain heart rate variability measures. Heart Rhythm 13: 1309–1316.

Sandrone G, Mortara A, Torzillo D, La Rovere MT, Malliani A, Lombardi F (1994). Effects of beta blockers (atenolol or metoprolol) on heart rate variability after acute myocardial infarction. Am J Cardiol 74: 340–345.

Sassi R, Cerutti S, Lombardi F, Malik M, Huikuri HV, Peng CK *et al.* (2015). Advances in heart rate variability signal analysis: joint position statement by the e-Cardiology ESC Working Group and the European Heart Rhythm. Association co-endorsed by the Asia Pacific Heart Rhythm Society. Europace 17: 1341–1353.

Task Force of the European Society of Cardiology and the North American Society of Pacing and Electrophysiology (1996). Heart rate variability: standards of measurement, physiological interpretation, and clinical use. Circulation 93: 1043–1065.

Tsuji H, Larson MG, Venditti FJ Jr, Manders ES, Evans JC, Feldman CL *et al*. (1996). Impact of reduced heart rate variability on risk for cardiac events. The Framingham Heart Study. Circulation 94: 2850–2855.

Supporting Information

Additional supporting information may be found online in the Supporting Information section at the end of the article.

https://doi.org/10.1111/bph.14354

Figure S1 Histograms of distribution of discrete mean values (i.e. 1 value per hour) over the entire circadian cycle (i.e. 24 values per animal/subject) of HFRR and HFHR oscillations in healthy human subjects ($n = 200$), beagle dogs ($n = 82$) and cynomolgus monkeys ($n = 77$). Animals were recorded in baseline conditions (treatment free recording period) for 24 h by telemetry. Solid blue line: normal curve. HFRRref and HFHRref are rounded values of the mean values calculated from all individual values of the entire distribution in each species.

Figure S2 Effect of atenolol (1 mg kg^{-1}, iv) on S1, S2 and S3 oscillations and on the HFAM ratio in cynomolgus monkeys. Black line: Dark period of the 12-hour-light/12- hour-dark cycle. Proportions in % $hour^{-1}$. Data are presented as mean values ± SEM ($n = 6$, *: $P \leq 0.05$ when compared to vehicle).

Figure S3 Effect of clonidine (0.1 mg kg^{-1}, iv) on S1, S2 and S3 oscillations and on the HFAM ratio in cynomolgus monkeys. Black line: Black line: Dark period of the 12- hour-light/12-hour-dark cycle. Proportions in % $hour^{-1}$. Data are presented as mean values ± SEM ($n = 6$, *: $P \leq 0.05$, when compared to vehicle).

Figure S4 Effect of atropine sulphate (1 mg kg^{-1}, iv) on S1, S2 and S3 oscillations and on the HFAM ratio in cynomolgus monkeys. Black line: Dark period of the 12- hour-light/12-hour-dark cycle. Proportions in % $hour^{-1}$. Data are presented as mean values ± SEM ($n = 6$, *: $P \leq 0.05$, when compared to vehicle).

Figure S5 Effect of atenolol (1 mg kg^{-1}, iv) on S1, S2 and S3 oscillations and on the HFAM ratio in beagle dogs. Black line: Dark period of the 12-hour-light/12-hour-dark cycle. Proportions in % $hour^{-1}$. Data are presented as mean values ± SEM ($n = 6$, *: $P \leq 0.05$, when compared to vehicle).

Figure S6 Effect of clonidine (0.1 mg kg^{-1}, iv) on S1, S2 and S3 oscillations and on the HFAM ratio in beagle dogs. Black line: Black line: Dark period of the 12-hourlight/ 12-hour-dark cycle. Proportions in % per hour. Data are presented as mean values ± SEM (n=6, *: $P \leq 0.05$, when compared to vehicle).

Figure S7 Effect of atropine methyl-nitrate (1 mg kg^{-1}, iv) on S1, S2 and S3 oscillations and on the HFAM ratio in beagle dogs. Black line: Dark period of the 12- hour-light/12-hour-dark cycle. Proportions in % per hour. Data are presented as mean values ± SEM (n=6, *: $P \leq 0.05$, when compared to vehicle).

Figure S8 Effect of dofetilide (1 mg kg^{-1}, po) on S1, S2 and S3 oscillations and on the HFAM ratio in beagle dogs. Black line: Dark period of the 12-hour-light/12-hour-dark cycle. Proportions in % per hour. Data are presented as mean values ± SEM (n=6, *: $P \leq 0.05$, when compared to vehicle).

Figure S9 Effect of haloperidol (3 mg kg^{-1}, po) on S1, S2 and S3 oscillations and on the HFAM ratio in beagle dogs. Black line: Dark period of the 12-hour-light/12-hour-dark cycle. Proportions in % per hour. Data are presented as mean values ± SEM (n=6, *: $P \leq 0.05$, when compared to vehicle).

Figure S10 Effect of cisapride (6 mg kg^{-1}, po) on S1, S2 and S3 oscillations and on the HFAM ratio in beagle dogs. Black line: Dark period of the 12-hour-light/12-hour-dark cycle. Proportions in % per hour. Data are presented as mean values ± SEM (n=6, *: $P \leq 0.05$, when compared to vehicle).

Figure S11 Proportions in % per hour. Effect of thioridazine (1.5 mg kg^{-1}, po) on S1, S2 and S3 oscillations and on the HFAM ratio in beagle dogs. Black line: Dark period of the 12-hour-light/12-hour-dark cycle. Proportions in % per hour. Data are presented as mean values ± SEM (n=6, *: $P \leq 0.05$, when compared to vehicle).

Figure S12 Circadian changes in heart rate in healthy subjects (n=200), cynomolgus monkeys (n=77) and beagle dogs (n=82). Black line: Dark period of the 12-hourlight/ 12-hour-dark cycle. Data are presented as mean values ± SEM (n=6).

Figure S13 Effect of atenolol (1 mg kg^{-1}, iv), clonidine (0.1 mg kg^{-1}, iv) and atropine sulphate (1 mg kg^{-1}, iv) on mean heart rate in cynomolgus monkeys. Black line: Dark period of the 12-hour-light/12-hour-dark cycle. Data are presented as mean values ± SEM (n=6, *: $P \leq 0.05$, when compared to vehicle).

Figure S14 Effect of atenolol (1 mg kg^{-1}, iv), clonidine (0.1 mg kg^{-1}, iv) and atropine methyl-nitrate (1 mg kg-1, iv) on mean heart rate in beagle dogs. Black line: Dark period of the 12-hour-light/12-hour-dark cycle. Data are presented as mean values ± SEM (n=6, *: $P \leq 0.05$, when compared to vehicle).

Figure S15 Effect of dofetilide (1 mg kg^{-1}, po), haloperidol (3 mg kg^{-1}, po), cisapride (6 mg kg^{-1}, po) and thioridazine (1.5 mg kg^{-1}, po) on mean heart rate in beagle dogs. Black line: Dark period of the 12-hour-light/12-hour-dark cycle. Data are presented as mean values ± SEM (n=6, *: $P \leq 0.05$, when compared to vehicle).